Photoionization of helium above the He+(n=2) threshold: Autoionization and final-state symmetry

D. W. Lindle, T. A. Ferrett, U. Becker,* P. H. Kobrin,†
C. M. Truesdale,‡ H. G. Kerkhoff,* and D. A. Shirley

*Materials and Molecular Research Division, Lawrence Berkeley Laboratory, Berkeley, California 94720
and Department of Chemistry, University of California, Berkeley, California 94720*

(Received 3 June 1983; revised manuscript received 17 October 1984)

The partial cross section, the satellite branching ratio, and the angular-distribution asymmetry parameter for simultaneous photoionization and excitation to the $n=2$ states of the He+ ion have been measured in the 67.5—90-eV photon-energy range. In the nonresonance regions (67.5 eV $\leq h\nu \leq$ 69.5 eV and 75 eV $\leq h\nu \leq$ 90 eV), the asymmetry-parameter values have been used to infer the ratio of the $2p$ cross section to the $2s$ cross section. These results indicate that the He+($n=2$) satellite is predominantly $2p$ near threshold, in agreement with the experimental and most of the theoretical results reported to date. In the region below the He+($n=3$) threshold (69.5 eV $\leq h\nu \leq$ 73.0 eV), the effects of a series of autoionizing Rydberg levels on the $n=2$ cross section, branching ratio, and asymmetry parameter have been measured, this being the first detailed measurement of the angular distribution of a satellite over an autoionization resonance. In addition, qualitative information concerning the total cross section and the $1s$ partial cross section has been obtained for the first member of this series ($3s3p$), disagreeing with previous experimental and theoretical results for the total cross section, but in agreement with recent photoemission measurements of the $1s$ cross section. The present results suggest that the qualitative shapes of the total and $1s$ cross sections over the $3s3p$ resonance are similar to the profile of the $n=2$ cross section for this resonance. To illustrate quantitative methods for the interpretation of autoionization phenomena, the derivation from the resonance data of several parameters defining the autoionization process is described.

I. INTRODUCTION

The photoionization of helium provides the simplest example of electron correlation in atomic physics. Because correlation cannot occur in the hydrogenlike final state, theoretical studies of initial-state and continuum-state correlation effects are easier to interpret for the photoionization process. For this reason helium is an important system for testing various theoretical approaches to the phenomenon of electron correlation. Past interest focused upon absolute cross-section measurements, as reviewed by Marr and West.[1] Theoretical calculations[2] of the total cross section, at least below the He+($n=2$) threshold, have proven to be very accurate. Recent interest[3-12] has centered upon the photoionization processes above this threshold, which can leave the residual He+ ion in the $2s$ or $2p$ excited states. Several calculations[13-19] of the partial photoionization cross section, the satellite and subshell branching ratios, and the angular-distribution asymmetry parameter have been performed for the He+($n=2$) states, indicating that much is still to be learned from this simple system about the influence of correlation on measurable quantities.

Figure 1 depicts the atomic and ionic states in helium relevant to this experiment. We have studied the photoionization processes

$$\text{He}(1s^2)+h\nu \rightarrow \text{He}^+(1s,2s,2p)+e^- \qquad (1)$$
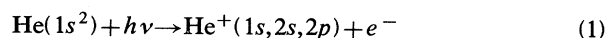
as a function of photon energy and photoelectron ejection angle. The He+($2s$) and He+($2p$) states are effectively degenerate in a photoemission experiment and thus comprise a single satellite line, which we designate He+($n=2$). We have measured the partial cross sections σ, and angular-distribution asymmetry parameters β, for the processes
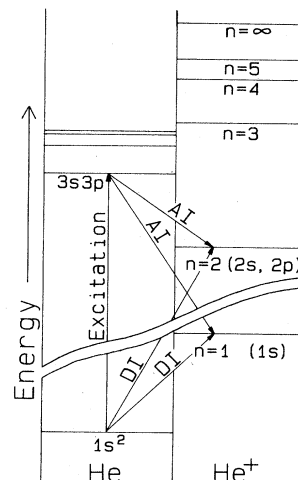

FIG. 1. Energy-level diagram for helium. DI is direct ionization. AI is autoionization. The energy scale above the break is expanded four times relative to the energy scale below the break.

represented in Eq. (1) that leave the He$^+$ ion in the 1s or the $n = 2$ final states, as well as the branching ratio $R_{21} = \sigma_{n=2}/\sigma_{1s}$, of the satellite intensity relative to that of the main line. The threshold for production of the $n = 2$ states from the ground state of the helium atom is 65.4 eV. We have taken photoelectron spectra for photon energies from 1.9 eV above this threshold to 90 eV. This energy range can be divided into resonance and nonresonance regions. In the resonance region it is possible to excite a series of Rydberg levels leading to the third ionization threshold at 73.0 eV with subsequent autoionization.

The nonresonance data, taken with photon energies in the ranges 67.5—69.5 and 75—90 eV, show good agreement with previous measurements[4,6—8,10,12] and calculations[13—19] of the partial cross sections for both the $n = 1$ and 2 final states [direct ionization (DI) processes in Fig. 1] and for the total (i.e., 2s plus 2p) satellite branching ratio. The ratio of the 2p cross section to the 2s cross section, R, which can be derived from $\beta_{n=2}$, provides a more sensitive test of theory. Discrepancies exist among the various experimental[9—12] and theoretical[14—19] values of R reported to date. Chang[16] has predicted that near threshold the 2s contribution to $\sigma_{n=2}$ is larger than that of the 2p level, in contrast to several other predictions.[14,15,17—19] Experimentally, the earliest photoemission data[9] were consistent with either calculation, but later photoemission[11,12] and fluorescence[10] measurements tended to discount Chang's prediction. Our results support the conclusion that the He$^+$($n = 2$) final state is predominantly 2p near threshold. The disagreement in the theoretical results indicates the need for a better understanding of the contributions of electron correlation to the photoionization process.

A different perspective on correlation can be obtained in the analysis of autoionization resonances. The interaction of various continuum-state wave functions with an excited Rydberg level determines the extent and profile of the autoionization process. We have taken photoelectron spectra in the region of the lowest four Rydberg levels leading to the He$^+$($n = 3$) ionization threshold at 73.0 eV. The four levels studied are indicated in the left-hand portion of Fig. 1. Large variations in $\sigma_{n=2}$ and $\beta_{n=2}$ were found at these resonances. Our measured variation in $\sigma_{n=2}$ agrees with the fluorescence data of Woodruff and Samson.[10] The detailed variation of $\beta_{n=2}$ over the autoionization resonances is presented here for the first time. In addition, we infer from our measurements that the qualitative shape of the total cross section over the first member of this Rydberg series differs with earlier experimental[20] and theoretical[21,22] results, but is consistent with recent photoemission data.[12]

The experimental procedures are described in Sec. II. The nonresonance data are presented in Sec. III, and the behavior of the cross sections, branching ratios, and asymmetry parameters over the autoionization resonances is discussed in Sec. IV. Conclusions are presented in Sec. V.

II. EXPERIMENTAL

Synchrotron radiation from the new 4° Grasshopper monochromator[23] at the Stanford Synchrotron Radiation

Laboratory (SSRL) was used to photoionize an effusive jet of helium atoms. The photoelectrons were detected at 0° and 54.7° with respect to the polarization vector of the photon beam by the double-angle time-of-flight (DATOF) method,[24] taking advantage of the pulsed time structure of the synchrotron radiation. This configuration allowed us to measure simultaneously the partial cross sections and angular-distribution asymmetry parameters for both the main and satellite lines of He$^+$.

The angular distribution of photoelectrons ejected from a randomly oriented sample by linearly polarized radiation, in the dipole approximation, is given by

$$\frac{d\sigma(h\nu,\theta)}{d\Omega} = \frac{\sigma(h\nu)}{4\pi}[1+\beta(h\nu)P_2(\cos\theta)] , \qquad (2)$$

where $h\nu$ is the photon energy, θ is the angle between the propagation vector of the photoelectron and the polarization vector of the ionizing radiation, $\sigma(h\nu)$ is the total cross section, $\beta(h\nu)$ is the asymmetry parameter that completely describes the angular distribution, and $P_2(\cos\theta)$ is the second Legendre polynomial. Photoelectron intensities measured at $\theta = 54.7°$, for which $P_2(\cos\theta)$ vanishes, are directly proportional to $\sigma(h\nu)$ after normalization to the photon flux and gas pressure. The measurement of photoelectron intensities at the additional angle of 0° suffices to determine values of $\beta(h\nu)$ that do not require such normalization. Calibration of the analyzers was accomplished by the measurement of the known partial cross sections and asymmetry parameters of the 2s and 2p levels of Ne$^+$.[25] This procedure is described in detail in Refs. 24 and 26, where it is shown that systematic errors are reduced significantly by this method. We estimate systematic errors to be ± 0.10 or less for measurement of asymmetry parameters and ± 10—15 % for cross sections and branching ratios. The calibration also effectively eliminates systematic errors due to nonlinear polarization of the radiation. In fact,[26] the polarization only need be greater than $\sim 70\%$. For this work it has been estimated to be 98%.[26]

The DATOF photoelectron spectrometer has been described previously.[27] It is ideally suited for studying low cross-section satellite lines, such as in helium, because of its high signal-to-noise ratio and its ability to collect many photoelectron energies simultaneously. Briefly, the experimental chamber was isolated from the ultrahigh-vacuum monochromator by a 1500-Å-thick aluminum window. The typical pressure in the interaction region was estimated to be 3 to 4×10^{-3} Torr. For partial cross-section measurements the sample pressure was monitored by a capacitance manometer and the photon flux by a sodium-salicylate scintillator and an optical photomultiplier tube (RCA 8850). Typical count rates for the He$^+$($n = 2$) satellite were 3—8/sec, with accumulation times of 1000 sec for each spectrum. An example of a time-of-flight spectrum for helium from the 54.7° detector is shown in Fig. 2.

III. NONRESONANCE PHOTOIONIZATION

Our measurement of the branching ratio R_{21} is shown in Fig. 3 along with several theoretical curves and other
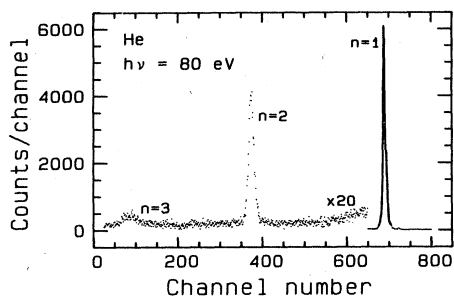
FIG. 2. TOF photoelectron spectrum of helium taken with the 54.7° detector at a photon energy of 80 eV. The peak labels indicate the principal quantum number of the single-electron final state of the ion.

experimental measurements. The value of R_{21} in the high-energy limit has been calculated[13,15] to be 4.8%, which can be compared to the values of 6(1)% at 190 (Ref. 6) and 278 eV[3] photon energy and 5.0(8)% for an Al $K\alpha$ measurement.[5] Our results in the near-threshold region show good agreement with previous measurements.[4,6,8] We see also that the available theoretical calculations[13-17] predict reasonably well the qualitative behavior of the branching ratio near threshold, although two of them[15,17] deviate from the measured values at the lowest energies. The calculations differ in that most of them,[13-16] including one of the errant curves,[15] contain a significant amount of configuration interaction (CI), while one[17] includes none at all, indicating that the ability to predict the energy dependence of R_{21} is dependent mostly on the *way* in which CI is included in the calculations. This also holds true when we consider the individual partial cross sections for the $2p$ and $2s$ final states. The measurement of these partial cross sections, or their ratio R, constitutes a more sensitive test of the theoretical calcula-
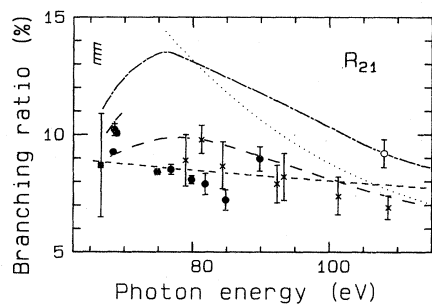
tions because the energy dependences of σ_{2p} and σ_{2s} are quite different.

Experimentally, two approaches have been taken. Woodruff and Samson[10] measured R directly by taking advantage of the long lifetime of $He^+(2s)$ to distinguish between fluorescence from the $2s$ and $2p$ levels. A second method, used by several groups[9,11,12] including ours, relies on the measurement of the asymmetry parameter $\beta_{n=2}$, which is a weighted average of β_{2s} and β_{2p}:

$$\beta_{n=2} = \frac{\sigma_{2s}\beta_{2s} + \sigma_{2p}\beta_{2p}}{\sigma_{2s} + \sigma_{2p}} . \quad (3)$$

By rearranging Eq. (3), and assuming that β_{2s} is always 2, R can be expressed in terms of $\beta_{n=2}$:

$$R = \frac{\sigma_{2p}}{\sigma_{2s}} = \frac{2 - \beta_{n=2}}{\beta_{n=2} - \beta_{2p}} . \quad (4)$$

This latter approach, of course, must rely on the calculated values of β_{2p}. Fortunately, the two available calculations[9,15] of β_{2p} behave similarly as a function of energy.

Our results for $\beta_{n=2}$ are presented in Fig. 4 along with the theoretical calculations[9,15] of $\beta_{n=2}$ and β_{2p}, and a curve representing a fit to all of the experimental results for $\beta_{n=2}$, including the present data, reported to date.[9-12] Figure 5 shows the values of R derived from the experimental data in Fig. 4 (our points and the fitted curve) and from the calculated values of β_{2p} from Jacobs and Burke.[15] Also shown are five calculations of R.[14-19] Approximately 75% of the experimental measurements represented by the solid curve in Fig. 4 are within ±0.1 of this curve, and greater than 90% are within ±0.2, indicating the good agreement among the five sets of data. However, agreement is poorer for R in Fig. 5 because Eq. (4) magnifies small differences between measured $\beta_{n=2}$ values into larger differences between inferred values of R. This effect can be observed by reference to the present
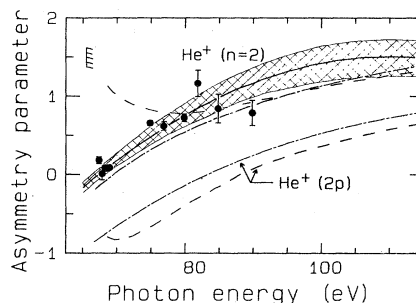

FIG. 3. Branching ratio $R_{21} = \sigma_{n=2}/\sigma_{1s}$ for the $He^+(n=2)$ satellite relative to the $1s$ main line. Experimental results: solid circles, present results; solid square, Samson, Ref. 4; open circle, Krause and Wuilleumier, Ref. 6; ×, Wuilleumier *et al.*, Ref. 8. Theoretical curves: short dashed, Salpeter and Zaidi, Ref. 13; dashed-dotted, Jacobs, Ref. 14; long-short dashed, Jacobs and Burke, Ref. 15; long dashed, Chang, Ref. 16; dotted, Richards, Ref. 17. Where applicable (Refs. 14—17) we have plotted only the velocity results for consistency.

FIG. 4. Asymmetry parameter of the $He^+(n=2)$ satellite. Experimental results: solid circles, present results; solid curve, second-order polynomial fitted to all of the available experimental data, Refs. 9—12 and the present results. Cross-hatched area represents ±1σ standard deviation about the fitted curve. Theoretical curves: long-short dashed, Jacobs and Burke, Ref. 15; dashed, Chang from Bizau *et al.*, Ref. 9. Also shown are calculations of the asymmetry parameter for the $2p$ final state by Jacobs and Burke (Ref. 15) and Chang (Ref. 9). The velocity forms of the calculations have been plotted in all cases.
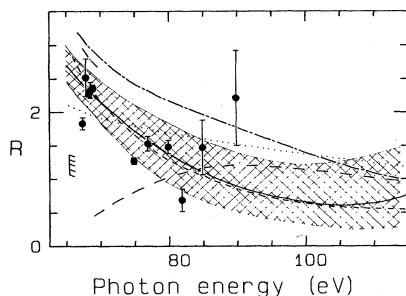
FIG. 5. The subshell branching ratio $R = \sigma_{2p}/\sigma_{2s}$ for the He$^+$(n =2) satellite. Experimental results: solid circles, present results; solid curve, derived from experimental curve in Fig. 4. The experimental values of R were determined from the $\beta_{n=2}$ measurements in Fig. 4 (solid circles and solid curve) and from β_{2p} calculated by Jacobs and Burke, Ref. 15 (lower long-short-dashed curve in Fig. 4), using Eq. (4). The cross-hatched region again represents $\pm 1\sigma$ standard deviation. Theoretical curves: dashed-dotted, Jacobs, Ref. 14; long-short dashed, Jacobs and Burke, Ref. 15; long-dashed, Chang, Ref. 16; dotted, Richards and Larkins, Ref. 19; short dashed, Berrington et al., Ref. 18. From Berrington et al. we show the length form of their calculation which the authors predict to be more accurate than the velocity form. The remainder of the curves are velocity forms.

results in Fig. 5. Consequently, caution must be exercised concerning detailed interpretation of the experimental curve for R (solid) because the data scatter considerably about this curve.

We wish to interpret the results in Fig. 5 in terms of initial-state and continuum-state configuration interaction (ISCI and CSCI, respectively). Configuration interaction in the hydrogenlike final state is not possible and does not need to be considered. For ISCI the initial state of the helium atom is written properly as an admixture of the $1s^2$, $1s\,2s$, $2s^2$, $2p^2$, and higher configurations. The ground state is predominantly $1s^2$, and we are interested in the degree to which any one of the other configurations mixes into the ground eigenstate. Similarly for CSCI, we are interested in the degree to which configurations such as $2s\epsilon p$, $2p\epsilon s$, and $2p\epsilon d$ mix with $1s\epsilon p$. We are aided in our interpretation by the fact that the energy-dependent cross sections of satellites whose origins are from ISCI or CSCI differ significantly.[28] Because initial-state mixing coefficients are essentially independent of energy, the relative intensities of ISCI-produced satellites will tend to be constant with energy. Conversely, because the photoelectron is included in the CSCI wave functions, we can expect the CSCI mixing coefficients, and hence the satellite cross sections, to be strongly energy dependent. Furthermore, it is known[28] that CSCI is most important near threshold, diminishing in significance at higher energies.

At photon energies above 100 eV, σ_{2s} is apparently the major component of $\sigma_{n=2}$. The slight upturn in R at the highest energies in Fig. 5 is probably an artifact of the relative scarcity of data above 110 eV. We therefore will interpret the results for R as if they approach a high-energy asymptotic value less than unity. In the high-energy limit we expect that only ISCI will contribute to the production

of the He$^+$(n =2) satellites.[28] For our assumed asymptotic value of R less than one we then conclude that ISCI favors the $2s$ satellite, implying that configurations of the form $2sns$ are more important for the ground state of the helium atom than the configurations $2pnp$. This may not be unexpected because the first group contains the configuration $1s\,2s$, which will mix well with $1s^2$ by virtue of the fact that it only differs by one electron and is closest in energy to the $1s^2$ configuration, whereas the $2pnp$ group has no such counterpart. Direct measurements[10] of σ_{2s} indicate that the ratio σ_{2s}/σ_{1s} is fairly constant for the first 60 eV above the $2s$ threshold, suggesting that the energy dependence of the He$^+$($2s$) satellite near threshold can be described well in terms of the ISCI formalism alone.

If ISCI were sufficient to describe the energy behavior of σ_{2p} as well, then R would remain less than unity at all energies. However, the results in Fig. 5 indicate a relative enhancement of σ_{2p} over σ_{2s} by approximately a factor of 4 as the threshold is approached. We attribute this rise to the influence of CSCI on the He$^+$($2p$) satellite and conclude that $2p\epsilon s$ and/or $2p\epsilon d$ are important configurations for the continuum state of He$^+$.

These qualitative conclusions about the importance of ISCI and CSCI to helium photoionization can be confirmed only after careful comparison to theoretical predictions. Quantitatively, the degree of predominance of one final state over the other and the applicable energy ranges can only be determined by theoretical calculations that accurately treat the effects of ISCI and CSCI. The goal is to gain information about the type and degree of CI present in the helium system, as well as general results concerning what treatments of CI are most reliable.

The theories used in the calculation of R differ significantly in sophistication. The calculation of Richards and Larkins[17,19] used Hartree-Fock (HF) wave functions in which the effects of relaxation have been included, but not CI. The calculation by Chang[16] also used HF wave functions, but included CI in both the initial state and the continuum states. Jacobs[14] and Jacobs and Burke[15] used a 56-term Hylleraas initial-state wave function, which is a nearly exact approximation of the He($1s^2$) ground state, and a close-coupling calculation for the final state, which is similar to CSCI. The calculation by Berrington et al.[18] is an improvement on the earlier close-coupling calculations in which care was taken to use the same configurations in the expansions for both the initial and continuum states. All of the calculations used final-state wave functions that are purely hydrogenic.

Above 90 eV all of the calculations show approximately the same behavior. Below 90 eV Chang's curve deviates signficantly from the rest and predicts a predominance of $2s$ near threshold. The experimental results show clearly that this is not correct, and we conclude that the $2p$ final state is the major component of He$^+$(n =2) at threshold, being more than twice as likely as the $2s$ final state. The calculation of Berrington et al. shows the best overall agreement with the combined experimental results.

The three close-coupling calculations (Jacobs, Jacobs and Burke, and Berrington et al.) and the calculation of Richards and Larkins behave similarly at low energy,

despite the fact that the latter is a much less sophisticated calculation. Richards and Larkins have concluded that CI and exchange are unimportant to their calculation except near threshold, and they cite this as the reason their calculation is qualitatively correct. Furthermore, they suggest[29] that the discrepancy in Chang's calculation may be the result of the use of CI wave functions that do not accurately take into account the direct interaction of the outgoing channels, which the other calculations do.[14,15,18] This ultimately may be the result of cancellation between large terms in the calculation of the transition amplitude.[16]

This example illustrates that much is still to be learned about the effects of CI on the calculation of the energy dependence of satellite cross sections. Except for isolated calculations on the Ne K shell,[30] the Li K shell,[17,19] and the valence shell of Fe,[31] the helium calculations are the only such theoretical studies completed to date. Helium thus appears to be a good candidate for further studies of electron-correlation effects in atomic photoionization.

At the photon energy of 80 eV (see Fig. 2), we were able to detect photoelectrons from the $He^+(n=3)$ final state. We determine its branching ratio relative to the main line R_{31} to be 1.8(2)% and its asymmetry parameter to be $-0.2(2)$. This value for R_{31} is in agreement with previous estimates[8,17,32] at this energy and the data of Bizau *et al.*[33] It also can be compared to the Al $K\alpha$ result of 1.4(8)%.[5] The negative value for $\beta_{n=3}$ indicates that the $3s$ final state is not the major component of this peak. In fact, the result of $-0.2(2)$ is consistent with the threshold value of -0.04 calculated by Greene,[34] who found approximately equal contributions from $3s$, $3p$, and $3d$.[35]

IV. RESONANCE PHOTOIONIZATION

Madden and Codling[36] first observed the Rydberg levels leading to the $n=3$ ionization threshold in helium in the energy range $69.5 \leq h\nu \leq 73.0$ eV. Of the five possible Rydberg series in this region, only one has been found to be significant. It is designated $(sp,3n+)^1P^o$, which is a positive admixture of $3snp\ ^1P^o$ and $3pns\ ^1P^o$. It has also been given[37] the configuration-mixed doubly excited symmetry-basis notation $K_n=1_n$, which we shall use here (except when the 1_3 resonance is discussed alone, to which we shall refer as the $3s\,3p$ resonance). The $(sp,3n-)^1P^o$ (or -1_n) series, the negative admixture of $3snp\ ^1P^o$ and $3pns\ ^1P^o$, has also been observed, but it is small enough to be neglected in the present analysis. The other possible $^1P^o$ series (with major component $3pnd$, $3dnp$, or $3dnf$) have not been observed.

The remainder of this section will deal with the analysis of the cross-section, branching-ratio, and asymmetry-parameter profiles over the 1_n series of resonances. To lay the groundwork for this analysis we begin (Sec. IV A) with a summary of several formalisms for describing autoionization phenomena. How these formalisms are used to fit the satellite data is discussed in Sec. IV B. Quantitative results for the cross section and branching ratio of the $n=2$ satellite are presented in Sec. IV C. From these results we have inferred qualitative information about the resonance profiles of σ_{1s} and the total cross

section σ_t. Resonance parameters are presented for σ_{1s} and σ_t with the proviso that the quantitative results are not very accurate, but are given to illustrate the usefulness of this type of analysis. To this end we determine several other parameters, including individual dipole matrix elements, to illustrate methods for the quantitative interpretation of an autoionization process. In Sec. IV D the $\beta_{n=2}$ resonance profile is discussed quantitatively and inferences for the ratio R in the resonance region are made.

A. Theoretical background

The effect of an isolated resonance, such as a Rydberg level, on the total photoabsorption or total photoionization cross section was derived originally by Fano.[38] The presence of a discrete level embedded in one or more continua causes an interference in the photon absorption process because of the indistinguishability of the two pathways, direct ionization and autoionization, leading to the final state. Fano derived the following expression for the total cross section σ_t for the case of a single discrete state interacting with one or more continuum states:

$$\sigma_t = \sigma_0 \left[\rho^2 \frac{(q+\epsilon)^2}{1+\epsilon^2} + 1 - \rho^2 \right] , \qquad (5a)$$

$$\epsilon = \frac{E-E_0}{\Gamma/2} , \qquad (5b)$$

where the Fano parameters q and ρ^2 are assumed constant over the resonance, σ_0 is the cross section far from the resonance, Γ and E_0 are the full width at half maximum (FWHM) and the position of the resonance, respectively, and ϵ is a reduced energy.

The quantities q, ρ^2, σ_0, and Γ can be expressed in terms of the dipole matrix elements for transitions from the ground state g to the discrete state ϕ, and to the continua μ, together with the Coulomb-interaction matrix elements coupling the discrete state to the continua. The q parameter, which governs the shape of the total cross section, is given by

$$q = \frac{\langle \Phi | \mathbf{r} | g \rangle}{\pi \sum_\mu \langle \phi | V | \mu \rangle \langle \mu | \mathbf{r} | g \rangle} , \qquad (6)$$

and the correlation coefficient ρ^2, which is a measure of the strength of the resonance, is given by

$$\rho^2 = \frac{\sum_\mu | \langle \phi | V | \mu \rangle \langle \mu | \mathbf{r} | g \rangle |^2}{\sum_\mu | \langle \phi | V | \mu \rangle |^2 \sum_\mu | \langle \mu | \mathbf{r} | g \rangle |^2} , \qquad (7)$$

where $\mathbf{r}$ and V represent the dipole and Coulomb operators, respectively, and Φ is the discrete state modified by an admixture of the continuum states. The degree to which Φ is different from ϕ is dependent upon the energy variations of the continuum wave functions in the vicinity of the resonance. The linewidth of the resonance is given by

$$\Gamma = 2\pi \sum_\mu | \langle \phi | V | \mu \rangle |^2 , \qquad (8)$$

and the nonresonance, background cross section is given by

$$\sigma_0 = \sum_\mu |\langle \mu | \mathbf{r} | g \rangle|^2 .$$ (9)

While the matrix elements in Eqs. (6) and (7) are not strictly energy independent, they are slowly varying functions of energy, and q and ρ^2 therefore are assumed to be constant in the vicinity of the resonance.

The Fano parametrization [Eqs. (5)—(9)] can explain the many different shapes measured for autoionization resonances. For example, the sign of the q parameter determines whether the resonance profile of the total cross section reaches its minimum on the low-energy side ($q > 0$) or the high-energy side ($q < 0$) of the resonance. This property will be referred to as the "phase" of the resonance profile. Other shapes can also be obtained from these expressions, such as a window resonance ($q = 0$) or a noninterfering Lorentzian peak added to the background cross section ($|q| \gg 0$).

The parametrization shown above is most applicable to the effect of an isolated resonance on the total photoabsorption cross section. In general, however, atomic Rydberg levels form a series whose members are not well-separated in energy and thus cannot be considered isolated. Equation (5a) is not easily adaptable to such a series of noninteracting, closely spaced resonances because the background cross section appears as a multiplicative factor for each resonance, making a simple summation unsatisfactory. Shore[39] has derived an equivalent expression that is better suited for a series of closely spaced resonances because it is mathematically simpler to work with. His expression is

$$\sigma_t = C + \sum_k \frac{B_k + A_k \epsilon_k}{1 + \epsilon_k^2} ,$$ (10)

where C is the background cross section for the series of resonances, the summation is over the k resonances, ϵ_k is as defined in Eq. (5b) for each resonance, and A_k and B_k are the shape parameters for the kth resonance, which we shall refer to as the "Shore parameters." The value C is understood to be a slowly varying function of the photon energy. As with the Fano parameters q and ρ^2, the Shore parameters A and B are assumed constant in the resonance region.

It is clear that for the case of a single isolated resonance, the Fano and Shore parametrizations can be expressed in the same mathematical form as follows:

$$\sigma_t = \sigma_0 \left[\frac{C_1 + C_2 \epsilon + \epsilon^2}{1 + \epsilon^2} \right] ,$$ (11)

where C_1 and C_2 can be expressed in terms of either q and ρ^2 or A and B. We note that although the Shore formalism is to be preferred for multiple resonances, the parameters A and B are not dimensionless quantities as are q and ρ^2. Because of this, the Fano formalism is more descriptive in the isolated-resonance case.

The formalisms presented so far were derived for the total cross section. In a photoemission experiment, however, partial cross sections commonly are measured.

Starace[40] has addressed the problem of several outgoing channels in the vicinity of an autoionization resonance. Davis and Feldkamp[41] and Combet Farnoux[42] have derived equivalent expressions. We shall use the notation of Starace. His expression for the partial cross section of each of the *observable* photoemission channels μ is

$$\sigma(\mu) = \frac{\sigma_0(\mu)}{1 + \epsilon^2} \{ \epsilon^2 + 2[q \, \mathrm{Re}(\alpha_\mu) - \mathrm{Im}(\alpha_\mu)] \epsilon + 1$$

$$- 2q \, \mathrm{Im}(\alpha_\mu) - 2 \, \mathrm{Re}(\alpha_\mu)$$

$$+ (q^2 + 1) |\alpha_\mu|^2 \} ,$$ (12)

where $\sigma_0(\mu)$ is the off-resonance partial cross section for the μth observable final state and ϵ and q are defined in Eqs. (5b) and (6), respectively. The complex parameter α_μ is given by[43]

$$\alpha_\mu = \frac{\langle \phi | V | \mu \rangle}{\langle g | \mathbf{r} | \mu \rangle} \left[\frac{2\pi}{\Gamma} \sum_\mu \langle g | \mathbf{r} | \mu \rangle \langle \mu | V | \phi \rangle \right] ,$$ (13)

with Γ given by Eq. (8). The term in large parentheses is common to all channels. The α_μ parameters can be thought of as replacing ρ^2 as the correlation coefficient for each channel when partial cross sections are measured. It is important to note that each μ represents an observable photoionization channel [e.g., $He^+(1s\epsilon p_{1/2})$]. This restriction was not necessary in the Fano and Shore derivations of the resonance behavior of the total cross section because the individual photoemission channels only appeared in summations over μ. It is clear that Eq. (12) has the same form as Eq. (11) because it describes the characteristic behavior of a cross section in the vicinity of an autoionization resonance. We will refer to $C_1(\mu)$ and $C_2(\mu)$ as the "Starace parameters."

Because all of the preceding formalisms, whether for total or partial cross sections, have the same mathematical form, it is possible to equate the parameters of the various formalisms, keeping in mind that expression of the parameters in terms of the appropriate matrix elements is only possible if the proper formalism for any given experiment is used. For example, although effective Fano parameters can be derived for the autoionization profile of a partial cross section, it may be misleading to report them as the appropriate resonance parameters because the expressions given by Fano for q and ρ^2 are not directly applicable to a partial cross section. They can be used in a descriptive context, however. This point will be discussed further in Sec. IV B.

An additional complication, discussed in Ref. 44, occurs because every peak m in a photoemission spectrum contains more than one of the channels μ such as the $He^+(1s)$ peak, which has contributions from two outgoing channels, $1s\epsilon p_{1/2}$ and $1s\epsilon p_{3/2}$.[45] Thus, the partial cross section for each photoelectron peak $\sigma(m)$ is the sum of several $\sigma(\mu)$. The expression for $\sigma(m)$ is of the same form as Eq. (12) but with $\sigma_0(\mu)$ replaced by the off-resonance partial cross section for the unresolved channels $\sigma_0(m)$, and $\mathrm{Re}(\alpha_\mu)$, $\mathrm{Im}(\alpha_\mu)$, and $|\alpha_\mu|^2$ replaced by $\mathrm{Re}\langle \alpha \rangle_m$, $\mathrm{Im}\langle \alpha \rangle_m$, and $\langle |\alpha|^2 \rangle_m$, which are averaged

quantities weighted by the $\sigma_0(\mu)$. The Schwartz inequality requires that

$$(\mathrm{Re}\langle\alpha\rangle_m)^2+(\mathrm{Im}\langle\alpha\rangle_m)^2\leq\langle\,|\,\alpha\,|^{\,2}\rangle_m \qquad (14)$$

so that the modified Eq. (12) contains three unknown quantities. Because a fit to the form of Eq. (11) only provides two parameters, it is, in general, impossible to solve for all three unknowns.

The angular-distribution asymmetry parameter β also can show effects of autoionization. Kabachnik and Sazhina[46] have shown that, for photoionization in the region of an isolated resonance, β is given by

$$\beta=\frac{X'\epsilon^2+Y'\epsilon+Z'}{A'\epsilon^2+B'\epsilon+C'} \ , \qquad (15)$$

where A', B', and C' are defined in terms of the parameters for the cross section over the resonance, and X', Y', and Z' are new parameters that depend on the same matrix elements presented earlier, as well as their relative phases. Equation (15) was obtained by the division of two functions of the form of Eq. (11).

The parameters in Eq. (15) have been expressed[46] in terms of the same dipole and Coulomb matrix elements used in the description of the resonance behavior of total and partial cross sections. The expressions derived by Kabachnik and Sazhina describe the resonance effect upon the asymmetry parameter β_t for the *total* photoelectron flux from a given sample. Except possibly for the special case of no interchannel coupling in the continuum, these expressions cannot describe the resonance behavior of the asymmetry parameter β_μ for an individual photoemission channel in terms of these matrix elements. This is especially true for helium because, as we have seen from the discussion in Sec. III, continuum interactions are important. While the form of Eq. (15) correctly describes these "partial β's," no detailed interpretation of the resulting parameters is yet possible.

B. Data analysis

In the present experiment the resonance behavior of the $\mathrm{He}^+(n=2)$ partial cross section, branching ratio, and asymmetry parameter in the region below the $n=3$ threshold was measured. The data for the $n=2$ satellite are shown in Figs. 6–8. The cross-section data were scaled to the absorption values given by Marr and West[1] at the off-resonance energy of 68.9 eV. The remainder of this section is devoted to a discussion of the fitting techniques and assumptions used to describe analytically the cross-section and asymmetry-parameter data in the resonance region.

The $\sigma_{n=2}$ data, shown in Fig. 6, were fitted to the Shore formula, Eq. (10), convoluted with a truncated triangular function of full width equal to 0.17 eV (0.43 Å) to account for monochromator broadening. The off-resonance cross section C was taken to be a linear function of energy. The positions E_0 and widths Γ of the four resonances were obtained from Woodruff and Samson.[10] The Shore parameters derived in this way are presented in Table I. Note that the values for the fourth resonance
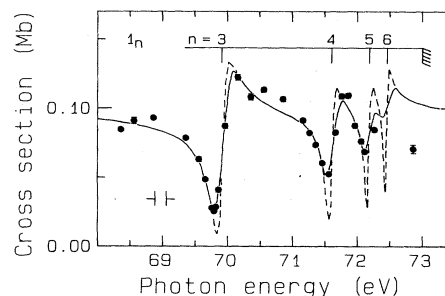

FIG. 6. Partial cross section of the $\mathrm{He}^+(n=2)$ satellite in the resonance region below the $n=3$ threshold scaled to Marr and West (Ref. 1) at 68.9 eV. The solid curve is a fit to the data using the form of Eq. (10). The dashed curve is the same fit with the monochromator broadening of 0.17 eV (0.43 Å) removed.

were held fixed. The solid curve in Fig. 6 shows this fit, whereas the dashed curve is the same fit but with the monochromator broadening removed.

The validity of using the Shore parametrization is dependent upon the assumption that the resonances are not coupled in any way, or equivalently, that the series of discrete levels ϕ_i do not perturb each other via Coulomb interactions. Shore[39] has indicated that this is a good approximation provided that the radiative widths of the resonance states are small compared to their overall widths. Typical radiative lifetimes for allowed dipole transitions are in the range 10^{-8}–10^{-9} sec,[47] so the radiative widths are several orders-of-magnitude smaller than the resonance widths.

The equivalent Starace parameters for $\sigma_{n=2}$ are also presented in Table I because they are the most interpretable parameters for a partial cross section. From the approximation in the previous paragraph we know that the Shore parameters derived from the fit to the $\sigma_{n=2}$ data represent isolated-resonance parameters and can be equated to the Starace parameters. Use of Eq. (10) in the present analysis is simply a mathematical construct to derive the appropriate Starace parameters.

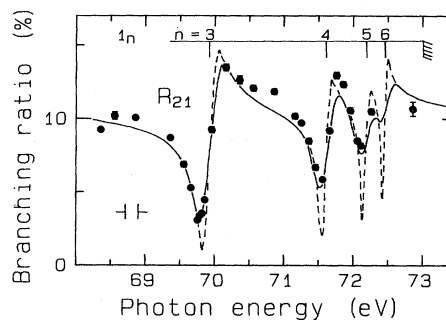The $n=2$ satellite branching ratio relative to the $1s$

FIG. 7. Branching ratio $R_{21}=\sigma_{n=2}/\sigma_{1s}$ for the $\mathrm{He}^+(n=2)$ satellite relative to the $1s$ main line in the resonance region below the $n=3$ threshold. The solid and dashed curves are fits to the data with and without monochromator broadening, respectively, as described in the text.
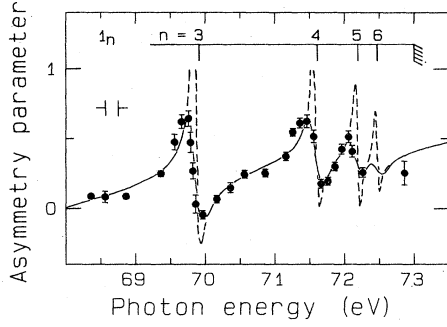
FIG. 8. Asymmetry parameter of the He$^+$(n =2) satellite in the resonance region below the n =3 threshold. The solid curve is a fit to the data using the form of Eq. (16). The dashed curve is the same fit with the monochromator broadening removed by the method described in the text.

main line (Fig. 7) also shows strong resonance effects, mainly due to the changes in $\sigma_{n=2}$. The branching-ratio data were fitted to a ratio of the two cross sections $\sigma_{n=2}$ and σ_{1s}, each written as in Eq. (10). The parameters for the function in the numerator were taken directly from the fit to $\sigma_{n=2}$. For the denominator σ_{1s} the background cross section was taken as a polynomial of first order in energy and the resonance parameters were varied to get the best fit. The numerator and denominator were convoluted separately with the same monochromator bandpass function used for the fit to the $\sigma_{n=2}$ data. The parameters for σ_{1s} for the $3s\,3p$ resonance from this fit can be found in Table II. The uncertainties in the σ_{1s} parameters for the higher-lying resonances derived from the branching-ratio fit are too large for these parameters to be reported with any confidence.

The asymmetry parameter for the n =2 satellite is affected strongly by autoionization because the peak includes contributions from two satellites with very different off-resonance asymmetry parameters. Our results are shown in Fig. 8. We have also measured β_{1s} in the resonance region and found it to be 2.00(5). The $\beta_{n=2}$ data were fitted in a manner identical to the fit to the branching-ratio data, except the parameters in the denominator were taken from the fit to $\sigma_{n=2}$ (Table I). The function used was

$$\beta_{n=2} = \frac{\displaystyle\sum_k \frac{Y_k + X_k \epsilon_k}{1 + \epsilon_k^2} + Z}{\displaystyle\sum_k \frac{B_k + A_k \epsilon_k}{1 + \epsilon_k^2} + C}.\tag{16}$$

The background value Z was assumed to be a second-order polynomial in energy. The resonance parameters X_k and Y_k are presented in Table III, where they have been used to determine X_k', Y_k', and Z_k' as in Eq. (15). The parameters A_k', B_k', and C_k' are not shown but can easily be derived from the values in Table I and Eqs. (15) and (16). We present these "Kabachnik-Sazhina parameters" for $\beta_{n=2}$, with the caveat that the definitions given in Ref. 46 do not allow easy interpretation for an individual photoemission line.

The fit to the $\beta_{n=2}$ data, including monochromator broadening, is shown in Fig. 8. The problem of deconvolution of instrumental broadening from the measured asymmetry parameters is not straightforward, especially if the monochromator bandpass is on the order of, or larger than, the resonance linewidth. The method used was the same as that described for the fit to R_{21}, but using Eq. (16). The method was chosen because the form of Eq. (16) is more amenable to fitting a series of closely spaced resonances and because the measured asymmetry parameters were derived from the ratio of peak intensities in two analyzers. The deconvoluted curve is shown in Fig. 8.

TABLE I. Parameters for the He$^+$(n =2) partial cross section for the first four members of the 1_n Rydberg series. The background cross section σ_0 was taken to be $0.216 - 0.0017E$ (eV) Mb, where E is the photon energy in eV. Numbers in parentheses represent statistical errors only.

| Resonance | | Shore parameters (Mb) | | | Starace parameters | |
		This work	WS[a]		This work	WS[a]
1_3	A	0.120(2)	0.081(14)	C_1	0.55(2)	0.24(11)
$E_0 = 69.917$ eV[a]	B	−0.044(2)	−0.065(8)	C_2	1.24(2)	0.94(18)
$\Gamma = 0.178$ eV[a]	C	0.097(1)	0.086(7)	σ_0 (Mb)	0.097(1)	0.086(7)
1_4	A	0.086(5)	0.079(17)	C_1	0.35(5)	0.23(13)
$E_0 = 71.601$ eV[a]	B	−0.061(5)	−0.066(10)	C_2	0.92(5)	0.92(21)
$\Gamma = 0.096$ eV[a]	C	0.094(1)	0.086(7)	σ_0 (Mb)	0.094(1)	0.086(7)
1_5	A	0.080(7)	0.088(21)	C_1	0.45(8)	0.49(15)
$E_0 = 72.181$ eV[a]	B	−0.051(7)	−0.044(12)	C_2	0.86(8)	1.02(26)
$\Gamma = 0.067$ eV[a]	C	0.093(1)	0.086(7)	σ_0 (Mb)	0.093(1)	0.086(7)
1_6	A	0.080 (fix)	0.085(28)	C_1	0.45(fix)	0.23(20)
$E_0 = 72.453$ eV[a]	B	−0.051(fix)	−0.066(16)	C_2	0.86(fix)	0.99(34)
$\Gamma = 0.038$ eV[a]	C	0.093(1)	0.086(7)	σ_0 (Mb)	0.093(1)	0.086(7)

[a]Woodruff and Samson, Ref. 10.

TABLE II. Parameters for the $He^+(1s)$ partial cross section for the $3s\,3p$ resonance. The background cross section σ_0 was taken to be $2.87-0.0283E$ (eV) Mb, where E is the photon energy in eV. Numbers in parentheses represent statistical errors only.

Effective Fano parameters[a]	Starace parameters[a]
$q=1.1(3)$	$C_1=1.01(3)$
$\rho^2=0.046(30)$	$C_2=0.10(7)$
$\sigma_0=0.892(20)$ Mb	$\sigma_0=0.892(20)$ Mb

[a]$E_0=69.917(12)$ eV and $\Gamma=0.178(12)$ eV from Ref. 10.

C. Results—cross sections and branching ratios

The parameters for $\sigma_{n=2}$ for the first four members of the Rydberg series leading to the $n=3$ threshold are listed in Table I, along with the results of Woodruff and Samson,[10] which agree with our results except for the $3s\,3p$ resonance. We attribute this small difference to the fact that the fit by Woodruff and Samson does not agree with their data for the first resonance quite as well as the fit presented here. The parameters for each member of the Rydberg series are fairly similar, as originally predicted by Fano and Cooper.[21] Results of several calculations[22,37,48-53] of these positions and widths are summarized in Ref. 10. Differences in the background cross sections (C and σ_0 in Table I) are due to differences in the scaling of the present data and the data in Ref. 10.

From the satellite branching ratio in Fig. 7 we have determined rough values of the σ_{1s} resonance parameters. Qualitatively we find that σ_{1s} has the same phase as $\sigma_{n=2}$ for the $3s\,3p$ resonance. Our qualitative, as well as quantitative (Table II), results are in complete agreement with recently published data for σ_{1s}.[12] Similarly, because σ_t is just the sum of σ_{1s} and $\sigma_{n=2}$, the total cross section also must have the same phase for this resonance. Quantitatively the situation for σ_t is summarized in Table IV. This qualitative interpretation for the phases of σ_{1s} and σ_t is in conflict with the phase of σ_{1s} over the $3s\,3p$ resonance required by the shape of σ_t as measured by Dhez and Ederer[20] together with the shape of $\sigma_{n=2}$ from the present results (the latter being in agreement with the fluorescence measurements of Woodruff and Samson[10] over the same region). The results from Dhez and Ederer

would require σ_{1s} and $\sigma_{n=2}$ to have opposite phases for this resonance because the effect on σ_t measured by them is small enough that the two partial cross sections must cancel when summed to yield the total cross section. This would require σ_{1s} to reach a maximum below the resonance energy and a minimum above that energy, a conclusion first reached by Woodruff and Samson[10] who based their conclusion on the result for σ_{1s} obtained by subtracting their $\sigma_{n=2}$ data from the σ_t data of Ref. 20. However, this conclusion is inconsistent with our results, as well as the direct measurement of σ_{1s}.[12] Because this cancellation does not occur, the strength of the effect on σ_t (as measured by ρ^2) must be significantly larger than that reported by Dhez and Ederer. This discrepancy might be explained by reference to Table I of Ref. 20 which lists the Shore parameters for the total cross section for a series of five transmission scans at three different pressures, 50, 90, and 120 Torr. Calculating q and ρ^2 for each scan shows a definite pressure dependence of ρ^2 (0.009 at 120 Torr, 0.013 at 90 Torr, and 0.018 at 50 Torr). Exactly what can cause such a pressure effect on ρ^2 is unclear.

Our value of q also disagrees with the previous result. While this may be due to our experimental uncertainties, it also could be the result of the normalization procedure used in the earlier work. By normalizing the data at 177.22 Å, which is an energy near the center of the resonance, that point is forced to lie on the background curve, fixing the shape of the resonance with respect to the background cross section and thus affecting q.

The present results are also to be compared with previous estimates of the resonance parameters. Fano and Cooper[21] estimated q and ρ^2 to be 1.7 and 0.01, respectively. Calculations by Senashenko and Wagué[22] using the diagonalization approximation yielded $q=1.31$ and $\rho^2=0.019$. Both of these calculations disagree with the larger value of ρ^2 inferred here. For the first estimate, however, it may be possible to trace one reason for this disagreement. In estimating q, Fano and Cooper assumed that the matrix elements involving the $1s\epsilon p$ continuum state for the $3s\,3p$ resonance are not significantly different than similar matrix elements for the $2s\,2p$ resonance. This assumption seems to imply, at least, that σ_{1s} has the same phase for both the $2s\,2p$ and the $3s\,3p$ resonances. However, σ_{1s} probably has opposite phases for these two resonances. The effect on the resulting values of q and ρ^2 for the total cross section is not clear. One other calcula-

TABLE III. Parameters for $\beta_{n=2}$ for the first four members of the 1_n Rydberg series. The background value Z was taken to be $2.28+0.0103E$ (eV)$-0.000\,61[E(\text{eV})]^2$ Mb, where E is the photon energy in eV. Numbers in parentheses represent statistical errors only.

Resonance	Fit parameters (Mb)			KS parameters (Mb)[a]		
	X	Y	Z	X'	Y'	Z'
1_3	$-0.030(6)$	$-0.037(5)$	$0.021(1)$	$0.021(1)$	$-0.030(6)$	$-0.016(5)$
1_4	$-0.031(9)$	$-0.037(9)$	$0.036(2)$	$0.036(2)$	$-0.031(9)$	$-0.001(9)$
1_5	$-0.031(14)$	$-0.040(14)$	$0.041(3)$	$0.041(3)$	$-0.031(14)$	$0.001(14)$
1_6	$-0.031(\text{fix})$	$-0.040(\text{fix})$	$0.043(3)$	$0.043(3)$	$-0.031(\text{fix})$	$0.003(\text{fix})$

[a]Kabachnik and Sazhina, Ref. 46.

TABLE IV. Parameters for the total cross section of helium for the $3s\,3p$ resonance derived from the results in Tables I and II. The numbers in parentheses represent statistical errors only.

| | Fano parameters | | Shore parameters (Mb) | |
	This work	DE[a]	This work	DE[a]
q	0.84(30)	1.36(20)	A 0.18(8)	0.032(6)
ρ^2	0.11(3)	0.012(3)	B −0.032(56)	0.010(5)
σ_0 (Mb)	0.989(20)	0.957(30)	C 0.989(20)	0.957(30)
Γ (eV)	0.178(12)[b]	0.132(14)		
E_0 (eV)	69.917(12)[b]	69.919(7)		

[a]Dhez and Ederer, Ref. 20.
[b]From Ref. 10.

tion[48] of σ_t for the $3s\,3p$ resonance has also been performed that reproduces the correct qualitative shape of the resonance, but no parameters were extracted because of the small number of points evaluated.

The remainder of this subsection will illustrate some of the quantitative results that can be derived from the measured parameters (Table I) and the parameters inferred for σ_{1s} and σ_t (Tables II and IV). We wish to stress that caution should be exercised concerning the actual values presented below, but the procedures described should prove to be useful in general for autoionization phenomena.

The oscillator strength f for the $3s\,3p$ resonance can be obtained from the Fano parameters for the total cross section. It is given by[54]

$$f = (0.195 \text{ Ry}^{-1}\text{Mb}^{-1})q^2\rho^2\sigma_t(\text{Mb})\Gamma(\text{Ry}) , \quad (17)$$

with Γ expressed in rydbergs and σ_t expressed in Mb. Using the values in Table IV we find $f = 2.0 \times 10^{-4}$, which agrees well with the previous estimate[21] of 1.2×10^{-4}. A similar but possibly more descriptive expression for f is obtained[55] by replacing q^2 in Eq. (17) with $(q^2 - 1)$. The result for this case is -8.1×10^{-5}, indicating that σ_t in the vicinity of the $3s\,3p$ resonance exhibits a net loss in oscillator strength compared to the background cross section. The latter value of f is more descriptive of autoionization in the sense that it is a measure of the spectral repulsion part of the autoionization profile.

Useful information also may be derived from the partial cross sections. Although, as we have pointed out, it is generally impossible to determine all three unknowns in Eq. (14), the simplicity of the helium system allows us to do so in a manner similar to the method described in an earlier paper.[44] The following discussion is limited to the $3s\,3p$ resonance, but similar results are expected for the higher-lying resonances. For He$^+$($1s$) production there

are only two outgoing channels μ, $1s\epsilon p_{1/2}$ and $1s\epsilon p_{3/2}$.[45] The dipole and Coulomb matrix elements for these two channels help determine two of the α_μ parameters, $\alpha_{1s\epsilon p_{1/2}}$ and $\alpha_{1s\epsilon p_{3/2}}$. Of course, both of these channels are present in the He$^+$($1s$) peak ($m = 1s$). In this case, however, because the spin-orbit interaction in the ϵp continuum is small, and because β_{1s} is identically 2.0 over the resonance, the Schwartz inequality, Eq. (14), becomes an equality. Equations (11), (12), and (14) and the Starace parameters in Table II may then be used to obtain $\text{Re}\langle\alpha\rangle_{1s}$, $\text{Im}\langle\alpha\rangle_{1s}$, and $\langle\,|\alpha|^2\rangle_{1s}$. The solution involves a complicated quadratic equation for $\text{Re}\langle\alpha\rangle_{1s}$. The solution with $\langle\,|\alpha|^2\rangle_{1s} > 2$ is dismissed because it would require that the total cross section have $\rho^2 > 1$. The parameters for the correct solution are given in Table V. These results also represent the nonaveraged quantities, $\text{Re}(\alpha_{1s\epsilon p_j})$, $\text{Im}(\alpha_{1s\epsilon p_j})$, and $|\alpha_{1s\epsilon p_j}|^2$, where j can have the values $\frac{1}{2}$ or $\frac{3}{2}$, because our earlier assumption that Eq. (14) is an equality means that the matrix elements of the dipole and Coulomb interactions for the two outgoing channels in the $1s$ peak are identical.

From Eqs. (15) and (16) in Ref. 44 we can determine the partial linewidths Γ_{1s} and $\Gamma_{n=2}$ for the two final states. Both of these partial widths are included in Table V. The large difference in the partial widths illustrates why the effect of the resonance on σ_{1s} is small relative to the effect on $\sigma_{n=2}$, even though $\sigma_0(1s)$ is an order-of-magnitude larger than $\sigma_0(n=2)$. The partial widths can be interpreted as an additional measure ($\langle\,|\alpha|^2\rangle_m$ is the other one) of the strength of the resonance effect on an individual final state. As we did with the α parameters for the $1s$ level, we can break down the contributions to Γ_{1s} into partial widths for each outgoing channel, being careful to account for the multiplicities of the two outgoing channels. The results are $\Gamma_{1s\epsilon p_{1/2}}/\Gamma = 0.004$ and $\Gamma_{1s\epsilon p_{3/2}}/\Gamma = 0.009$. The partial widths (in percent) de-

TABLE V. α parameters and partial linewidths for the $3s\,3p$ resonance.

Final state	$\text{Re}\langle\alpha\rangle_m$	$\text{Im}\langle\alpha\rangle_m$	$\langle\,|\alpha|^2\rangle_m$	$(\Gamma_m/\Gamma)\times 100$
$1s\epsilon p$	0.023(21)	−0.03(4)	0.0016 $\begin{array}{c}+0.0020\\-0.0016\end{array}$	1.3 $\begin{array}{c}+1.7\\-1.3\end{array}$
$\left.\begin{array}{l}2s\epsilon p\\2p\epsilon d\end{array}\right\}n=2$	0.99(15)	0.2(3)	1.1(3)	98.7 $\begin{array}{c}+1.3\\-1.7\end{array}$

rived here agree very well with previous calculations.[22,37]

Because we have already found $\langle |\alpha|^2 \rangle_{1s}$, we can use Eq. (17) in Ref. 43 to find $\langle |\alpha|^2 \rangle_{n=2}$. Having done this, $C_1(n=2)$ and $C_2(n=2)$ for the $3s\,3p$ resonance from Table I can be used with Eqs. (11) and (12) to find $\mathrm{Re}\langle\alpha\rangle_{n=2}$ and $\mathrm{Im}\langle\alpha\rangle_{n=2}$. These values are also presented in Table V. We note that for the α parameters for $\sigma_{n=2}$, Eq. (14) appears to be a true inequality. Because the satellite peak containing the $2s$ and $2p$ final states includes seven possible outgoing channels, no further information can be obtained.

A check of the α_μ parameters can be made as described in Ref. 44. The results in Table V satisfy this check to well within the statistical errors, suggesting that no major systematic errors are present in the data analysis.

Some interpretation of the α_μ parameters can be made, keeping in mind that the actual values may not be very accurate. The positive values of $\mathrm{Re}\langle\alpha\rangle_m$ for both the $1s$ and $n=2$ levels indicate that these two resonance profiles should have the same phase over the resonance, as we have suggested. The values for $\mathrm{Im}\langle\alpha\rangle_{1s}$ and $\mathrm{Im}\langle\alpha\rangle_{n=2}$ are zero within the estimated errors, showing that the α_μ parameters may be essentially real numbers. If this is true, the result seems fortuitous because it probably does not imply, as discussed by Combet Farnoux,[42] that interchannel coupling in the continuum is weak. In fact, because the $n=2$ peak is a satellite of the $1s$ peak, interchannel coupling in this case is important (see Sec. III). It might prove interesting to measure the α parameters for the individual final states $2s$ and $2p$. The strong coupling between $2s\epsilon p$ and $2p\epsilon s$ may result in α parameters that are complex. A detailed fluourescence experiment, similar to that done by Woodruff and Samson,[10] could measure these parameters.

To this point we have only derived parameters which depend on several of the dipole and Coulomb matrix elements. It is possible, however, for the case of the $3s\,3p$ resonance to determine directly the squares of three of the matrix elements, including all of those describing autoionization into the $1s\epsilon p$ continuum. The Coulomb matrix elements $|\langle 3s\,3p\,|\,V\,|\,1s\epsilon p_j\rangle|^2$, with $j=\frac{1}{2}$ or $\frac{3}{2}$, can be obtained from Eq. (8) for the partial decay width $\Gamma_{1s}=0.0023$ eV, by properly accounting for the multiplicity of the $1s\epsilon p_j$ states. The dipole matrix elements for continuum absorption, $|\langle 1s\epsilon p_j\,|\,\mathbf{r}\,|\,1s^2\rangle|^2$, can be determined from σ_{1s} as described in Ref. 21 and again consid-

ering the multiplicities. The dipole matrix elements also can be expressed as oscillator strengths. The dipole matrix element for the discrete transition $1s^2\rightarrow 3s\,3p$ can be determined[21] from the oscillator strength f derived above. All of these results are listed in Table VI along with estimates of two of the matrix elements by Fano and Cooper.[21] Their results agree with ours to within a factor of 2. One additional parameter can also be derived. The square of the term in brackets in Eq. (14) can be determined by using $\langle |\alpha|^2 \rangle_{1s}$ from Table V and the matrix elements in Table VI. We find this term to have the value 36 Mb/Ry^2.

Let us summarize the results of this subsection. Quantitatively we have presented parameters defining the resonance profiles of $\sigma_{n=2}$ and R_{21}. From these results we have inferred the *qualitative* behavior of σ_{1s} and σ_t for the $3s\,3p$ resonance only, concluding that the phases for $\sigma_{n=2}$, σ_{1s}, and σ_t are the same for this resonance. This result agrees with recent photoemission data but disagrees with an earlier photoabsorption measurement. Exercising caution for the quantitative results we have determined parameters that quantify the qualitative behavior of σ_{1s} and σ_t in order to illustrate methods for extracting information from measurements of autoionization phenomena. The results, such as α parameters and dipole matrix elements, which are obtained in this way can be useful in describing the aspects of interchannel coupling in the continuum[42] and for comparison with theoretical calculations of resonance behavior. Values for individual matrix elements may prove particularly helpful as a guide to determining appropriate wave functions and other parameters for calculations. As a final point we again wish to stress that while the results of this experiment are not sufficiently accurate to provide a complete and quantitative interpretation, we have attempted to document fully one of the first measurements of this kind.

D. Results—asymmetry parameters

The data in Fig. 8 mark the first detailed measurement of a satellite asymmetry parameter over autoionization resonances. The accompanying parameters in Table III vary only slightly over the members of the Rydberg series, as first predicted by Dill.[56]

Because the angular distributions of all the helium photoemission peaks (there are only two) were measured in this experiment, it is possible to determine β_t from

$$\beta_t = \frac{\beta_{1s} + R_{21}\beta_{n=2}}{1 + R_{21}} , \qquad (18)$$

with $\beta_{1s}=2$, and R_{21} and $\beta_{n=2}$ given by Eqs. (11) and (16) for the $3s\,3p$ resonance only. The resulting β_t has the same mathematical form as $\beta_{n=2}$, and the Kabachnik-Sazhina parameters describing it are given in Table VII. The off-resonance value of β_t is approximately 1.8, with deviations due to autoionization of only ~ 0.1, as expected because the dominant $1s$ channel shows no effect in β_{1s}. It is hoped that these results, as well as those for $\beta_{n=2}$, will spur further theoretical development regarding the detailed behavior of angular distributions of individual photoemission lines in the vicinity of autoionization reso-

TABLE VI. Matrix elements for the $3s\,3p$ resonance.

Matrix element	Amplitude	
	This work	Fano and Cooper (Ref. 21)
$\|\langle 3s\,3p\,\|\,\mathbf{r}\,\|\,1s^2\rangle\|^2$	1.1×10^{-3} Mb	6.8×10^{-4} Mb
$\|\langle 1s\epsilon p_j\,\|\,\mathbf{r}\,\|\,1s^2\rangle\|^{2\mathrm{a,b}}$	0.10 Mb/Ry	
$\|\langle 3s\,3p\,\|\,V\,\|\,1s\epsilon p_j\rangle\|^{2\mathrm{b}}$	4.5×10^{-6} Ry	4.7×10^{-6} Ry$^{\mathrm{c}}$

[a]The corresponding oscillator strength df/dE is 0.0014 eV^{-1}. [b]$j=\frac{1}{2}$ and $\frac{3}{2}$. [c]The value given by Fano and Cooper is for the sum over all the channels contributing to the $1s$ peak. We have divided their value by 6 for comparison.

TABLE VII. Kabachnik-Sazhina parameters for the angular distribution of the total photoelectron flux from helium for the $3s\,3p$ resonance. The numbers in parentheses represent statistical errors only.

$X'=1.81(4)$	$A'=0.99(2)$
$Y'=0.15(13)$	$B'=0.18(8)$
$Z'=1.79(7)$	$C'=0.96(6)$

nances. Complete understanding of this phenomenon awaits further theoretical and experimental work.

In Sec. III we were able to derive the ratio $R=\sigma_{2p}/\sigma_{2s}$ from the measured off-resonance $\beta_{n=2}$ data and calculated values of β_{2p}. We are unable to do this in the resonance region because the resonance behavior of β_{2p} is unknown, but certain qualitative statements can be made concerning the effects on R of the $3s\,3p$ resonance. For the following discussion the reader is referred to the deconvoluted curves in Figs. 6 and 8.

Figure 6 shows that the $n=2$ partial cross section drops nearly to zero at the minimum of the $3s\,3p$ resonance. From Fig. 5 the background value of R at 70 eV is ~ 2.2. Thus, to account for the minimum in $\sigma_{n=2}$, both σ_{2p} and σ_{2s} must be going through a minimum at the energy of the minimum in $\sigma_{n=2}$. Furthermore, both of these minima occur on the low-energy side of the $3s\,3p$ resonance. In other words, we can conclude that both σ_{2p} and σ_{2s} are effected by the resonance and that they have the same phase. The question then arises of whether or not these effects manifest themselves in an effect on R. If R is left unaffected, then the measured change in $\beta_{n=2}$ [see Eq. (3)] must be due solely to changes in β_{2p} (assuming that β_{2s} is always 2.0, just like β_{1s}). However, examination of the minimum in $\beta_{n=2}$ on the high-energy side of the resonance shows that even if β_{2p} is -1 at this energy, a value of $R=2.2$ is not large enough to yield [see Eq. (4)] the deconvoluted value of $\beta_{n=2}=-0.25$ from Fig. 8. The values of $R=2.2$ and $\beta_{2p}=-1$ yield $\beta_{n=2}=-0.06$. The uncertainty in the minimum of the deconvoluted curve for $\beta_{n=2}$ is ~ 0.1. Therefore, our value of $\beta_{n=2}=-0.25$ suggests that R shows a positive deviation from its background value of 2.2 on the high-energy side of the $3s\,3p$ resonance. Because R must have the shape of a branching ratio over an autoionization resonance, it must reach a minimum on the low-energy side of the $3s\,3p$ resonance as well. No limits can be placed on the value of this minimum. The conclusion then is that R drops to a minimum on the low-energy side and rises to a maximum on the high-energy side of the $3s\,3p$ resonance. This behavior is most likely caused by σ_{2p} and σ_{2s} having similar profiles, but with σ_{2p} reaching its minimum at a slightly lower energy than σ_{2s}. This implies that the Starace parameters $C_1(2p)$ and $C_2(2p)$ are slightly larger than $C_1(2s)$ and $C_2(2s)$, respectively. We expect the higher members of this series to have similar effects on R because partial cross sections tend to retain the same shape over a Rydberg series.[21]

V. CONCLUSIONS

The photoionization of helium to the $n=2$ excited state of the helium ion has provided several interesting results. The off-resonance measurements of $\beta_{n=2}$ have shown additional clear evidence that the $n=2$ satellite is mainly comprised of the $2p$ final state near threshold. Furthermore, the strong energy dependence of R has given some insight into the understanding of electron correlation in atomic systems, the helium case being especially useful because of its relative simplicity.

For the He$^+$($n=2$) satellite the partial cross-section, branching-ratio, and asymmetry-parameter behavior have been measured over the major Rydberg series leading to the $n=3$ threshold. These angular-distribution measurements are the first of their kind for a satellite line. Parameters describing all of these resonance effects have been presented. From the angular-distribution results the qualitative behavior of R over the resonances has been inferred.

The qualitative behavior of the total and $1s$ cross sections has been determined for the $3s\,3p$ resonance. The results have mixed agreement with previous measurements, and more work at higher resolution on the total cross section of helium above the $n\geq 2$ thresholds is recommended to verify our conclusions. The $1s$ cross-section results have been used in an illustrative way to indicate how information about autoionization behavior in photoemission can be extracted.

---

*Permanent address: Fachbereich Physik, Technische Universität Berlin, D-1000 Berlin 12, West Germany.

†Present address: Rockwell Science Center, P.O. Box 1085, Thousand Oaks, CA 91360.

‡Present address: Research and Development Division, Corning Glass Works, Corning, NY 14831.

[1]G. V. Marr and J. B. West, At. Data Nucl. Data Tables **18**, 497 (1976).

[2]G. Wendin, J. Phys. B **4**, 1080 (1971); T. Ishihara and R. T. Poe, Phys. Rev. A **6**, 116 (1972); M. Y. Amusia, N. A.

Cherepkov, D. Zivanović, and V. Radojević, *ibid.* 13, 1466 (1976).

[3]T. A. Carlson, Phys. Rev. 156, 142 (1967).

[4]J. A. R. Samson, Phys. Rev. Lett. 22, 693 (1969).

[5]T. A. Carlson, M. O. Krause, and W. E. Moddeman, J. Phys. (Paris) Colloq. 32, C4-76 (1971).

[6]M. O. Krause and F. Wuilleumier, J. Phys. B 5, L143 (1972).

[7]P. R. Woodruff and J. A. R. Samson, Phys. Rev. Lett. 45, 110 (1980).

[8]F. Wuilleumier, M. Y. Adam, N. Sandner, and V. Schmidt, J. Phys. (Paris) Lett. 41, L373 (1980).

[9]J. M. Bizau, F. Wuilleumier, P. Dhez, D. L. Ederer, T. N. Chang, S. Krummacher, and V. Schmidt, Phys. Rev. Lett. 48, 588 (1982).

[10]P. R. Woodruff and J. A. R. Samson, Phys. Rev. A 25, 848 (1982).

[11]V. Schmidt, H. Derenbach, and R. Malutzki, J. Phys. B 15, L523 (1982).

[12]P. Morin, M. Y. Adam, I. Nenner, J. Delwiche, M. J. Hubin-Franskin, and P. Lablanquie, Nucl. Instrum. Methods 208, 761 (1983).

[13]E. E. Salpeter and M. H. Zaidi, Phys. Rev. 125, 248 (1962).

[14]V. Jacobs, Phys. Rev. A 3, 289 (1971).

[15]V. L. Jacobs and P. G. Burke, J. Phys. B 5, L67 (1972).

[16]T. N. Chang, J. Phys. B 13, L551 (1980).

[17]J. A. Richards, Honours Thesis, Monash University, Australia, 1981.

[18]K. A. Berrington, P. G. Burke, W. C. Fon, and K. T. Taylor, J. Phys. B 15, L603 (1982); see P. C. Ojha, *ibid.* 17, 1807 (1984) for additional discussion of these calculations.

[19]J. A. Richards and F. P. Larkins, J. Electron Spectrosc. 32, 193 (1983).

[20]P. Dhez and D. L. Ederer, J. Phys. B 6, L59 (1973).

[21]U. Fano and J. W. Cooper, Phys. Rev. 137, A1364 (1965).

[22]V. S. Senashenko and A. Wagué, J. Phys. B 12, L269 (1979).

[23]F. C. Brown, R. Z. Bachrach, and N. Lien, Nucl. Instrum. Methods 152, 73 (1978).

[24]S. H. Southworth, C. M. Truesdale, P. H. Kobrin, D. W. Lindle, W. D. Brewer, and D. A. Shirley, J. Chem. Phys. 76, 143 (1982).

[25]F. Wuilleumier and M. O. Krause, J. Electron Spectrosc. 15, 15 (1979).

[26]S. H. Southworth, U. Becker, C. M. Truesdale, P. H. Kobrin, D. W. Lindle, S. Owaki, and D. A. Shirley, Phys. Rev. A 28, 261 (1983).

[27]M. G. White, R. A. Rosenberg, G. Gabor, E. D. Poliakoff, G. Thornton, S. H. Southworth, and D. A. Shirley, Rev. Sci. Instrum. 50, 1268 (1979).

[28]S. T. Manson, J. Electron Spectrosc. 9, 21 (1976).

[29]J. A. Richards and F. P. Larkins (private communication).

[30]T. Ishihara, J. Mizuno, and T. Watanabe, Phys. Rev. A 22, 1552 (1980).

[31]H. P. Kelly, Phys. Rev. A 6, 1048 (1972).

[32]R. L. Brown, Phys. Rev. A 1, 341 (1970).

[33]J. M. Bizau, F. J. Wuilleumier, D. L. Ederer, P. Dhez, S. Krummacher, and V. Schmidt (unpublished).

[34]C. H. Greene, Phys. Rev. Lett. 44, 869 (1980).

[35]C. H. Greene (private communication).

[36]R. P. Madden K. Codling, Astrophys. J. 141, 364 (1965).

[37]D. R. Herrick and O. Sinanoğlu, Phys. Rev. A 11, 97 (1975).

[38]U. Fano, Phys. Rev. 124, 1866 (1961).

[39]B. W. Shore, Phys. Rev. 171, 43 (1968).

[40]A. F. Starace, Phys. Rev. A 16, 231 (1977).

[41]L. C. Davis and L. A. Feldkamp, Phys. Rev. B 15, 2961 (1977); 23, 6239 (1981).

[42]F. Combet Farnoux, Phys. Rev. A 25, 287 (1982).

[43]P. C. Kemeny, J. A. R. Samson, and A. F. Starace, J. Phys. B 10, L201 (1977).

[44]P. H. Kobrin, U. Becker, S. Southworth, C. M. Truesdale, D. W. Lindle, and D. A. Shirley, Phys. Rev. A 26, 842 (1982).

[45]Although the $1s\epsilon p_{1/2}$ and $1s\epsilon p_{3/2}$ final states are not resolved in this work, they have to be considered here for the later discussion because of their different multiplicities.

[46]N. M. Kabachnik and I. P. Sizhina, J. Phys. B 9, 1681 (1976).

[47]G. Herzberg, *Molecular Spectra and Molecular Structure I. Spectra of Diatomic Molecules* (Van Nostrand, New York, 1950).

[48]S. Ormonde, W. Whitaker, and L. Lipsky, Phys. Rev. Lett. 19, 1161 (1967).

[49]P. G. Burke and A. J. Taylor, J. Phys. B 2, 44 (1969).

[50]R. S. Oberoi, J. Phys. B 5, 1120 (1972).

[51]K. T. Chung and I. Chen, Phys. Rev. Lett. 28, 783 (1972).

[52]Y. K. Ho, J. Phys. B 12, 387 (1979).

[53]Y. K. Ho, J. Phys. B 15, L691 (1982).

[54]U. Fano and J. W. Cooper, Rev. Mod. Phys. 40, 441 (1968).

[55]P. G. Burke and D. D. McVicar, Proc. Phys. Soc. (London) 86, 989 (1965).

[56]D. Dill, Phys. Rev. A 7, 1976 (1973).